Disentangling Projected Stationary Wave Changes: Implications for Future Drying of the Mediterranean Region

Benny Keller[a,b] Chaim I Garfinkel[a] Edwin P. Gerber[c]

[a] *The Hebrew University of Jerusalem, Institute of Earth Sciences, Edmond J. Safra Campus, Givat Ram, Jerusalem, Israel*

[b] *Atmospheric, Oceanic and Planetary Physics, Department of Physics, University of Oxford, Oxford, United Kingdom*

[c] *Courant Institute of Mathematical Sciences, New York University, New York, New York*

Corresponding author: Benny Keller, benjamin.keller@new.ox.ac.uk

ABSTRACT: An intermediate-complexity general circulation model is used to disentangle changes in the large-scale zonally asymmetric circulation in response to rising greenhouse gases. Particular focus is on the anomalous ridge that develops over the Mediterranean in future projections, directly associated with reduced winter precipitation over the region. Specifically, we examine stationary wave changes forced by land-sea contrast, zonal oceanic heat-fluxes, and orography, following a quadrupling of CO_2. The stationary waves associated with these three drivers depend strongly on the climatological state, precluding a linear decomposition of their responses to warming. However, our modelling framework still allows a process-oriented approach to quantify the key drivers and mechanisms of the response. A combination of three similarly important mechanisms is found responsible for the rain-suppressing ridge. The first is part of a global response to warming: elongation of intermediate-scale stationary waves in response to strengthened subtropical winds aloft, previously found to account for hydroclimatic changes in south-western North America. The second is regional: a downstream response to the North Atlantic warming hole and enhanced warming of the Eurasian landmass relative to the Atlantic Ocean. A third contribution to the Mediterranean ridge is a phase shift of planetary wave 3, primarily associated with an altered circulation response to orographic forcing. Reduced land-sea contrast in the Mediterranean basin, previously thought to contribute substantially to Mediterranean drying, has negligible effect in our integrations. This work offers a mechanistic analysis of the large-scale processes governing projected Mediterranean drying, lending increased understanding and credibility to climate model projections.

1. Introduction

Changes in regional precipitation and hydro-climate are among the most impact-relevant aspects of global warming. Rising temperatures are expected to cause a zonal mean drying of the subtropical dry regions and wetting of the tropical and mid-to-high-latitude wet regions, as atmospheric moisture holding capacity increases (Held and Soden 2006) and moisture transport intensifies (Seager et al. 2010). This zonal mean pattern, however, is not representative of conditions in any specific region. The precipitation response varies strongly with longitude, due to the strong zonal structure of storm tracks and stationary waves, i.e., the time-mean zonal deviations from the zonal mean flow, and their associated quasi-stationary highs and lows. This zonal structure is particularly pronounced in the Northern Hemisphere (Simpson et al. 2014). Uncertainty in the projected response of stationary waves to increased CO2 leads to large multi-model spread in precipitation projections in the extra-tropics (Brandefelt and Körnich 2008; Neelin et al. 2013; Garfinkel et al. 2020a). Therefore, accurate future precipitation projection in these water-stressed regions depends greatly upon an improved understanding of the mid-latitude large-scale circulation response to warming, and upon the ability of models to resolve key processes driving the change.

The Mediterranean region has been termed a climate change 'hot spot' (Giorgi 2006; Cos et al. 2022) due to its particular sensitivity to rising concentrations of greenhouse gasses (GHGs) in global climate models (GCM's). As GHGs concentrations rise, models project, with strong agreement, a large and zonally pronounced decrease in winter precipitation in the Mediterranean basin, particularly in the south-east of the region (Giorgi and Lionello 2008; Garfinkel et al. 2020a). The large reduction in precipitation in the region is associated with another climate feature projected robustly across GCM's: the formation of an anomalous surface anticyclone over the Mediterranean basin in winter months, accompanied by an upper level ridge (Giorgi and Lionello 2008). The magnitude of the surface anticyclone is strongly correlated with the regional winter precipitation decline across CMIP5 models (Zappa et al. 2015b).

It has long been assumed that the anomalous winter Mediterranean high drives the projected drying by increasing atmospheric stability in the region and suppressing Mediterranean cyclones (Giorgi and Lionello 2008). Brogli et al. (2019) found that, as opposed to summer drying, the decrease in precipitation over the Mediterranean in winter months is projected only when circulations changes are included. Zappa et al. (2015a) found that future Mediterranean drying is strongly related to a decrease in the number of Mediterranean cyclones, further amplified in the eastern Mediterranean by a reduction in the amount of precipitation generated by individual cyclones. In addition Armon et al. (2022) showed that future heavy rainfall events in the eastern Mediterranean will yield reduced rainfall, mainly due to a decrease in rain area, despite increased rain rate. Yet the question remains as to why the anomalous rain-suppressing high pressure develops in the first place, and this is the subject of our study.

After reviewing key mechanisms possibly relevant for Mediterranean drying in the literature (section 2), the simulation environment and experiments performed in this study are introduced in section 3. The results of our experiments and the role of individual stationary wave forcings for projected Mediterranean drying are then presented in section 4. A wavenumber decomposition and process-oriented assessment of the circulation response to warming are shown in section 5. Finally, the various mechanisms explaining winter Mediterranean drying are re-evaluated in light of our results in section 6, and our conclusions are summarized in section 7.

2. Background and theory

Various large-scale circulation changes have been proposed as drivers of the Mediterranean drying, including a weakening of the Mediterranean storm track (Lionello and Giorgi 2007; Zappa et al. 2015a) and a poleward shift of the Hadley cell associated with a corresponding shift of the North Atlantic storm track (Scheff and Frierson 2012). As yet, a satisfactory and universally accepted explanation has yet to be found. The Hadley cell and storm-track shifts occur on a faster time scale than the projected precipitation decrease in the Mediterranean (He and Soden 2017), and the inter-model spread in zonal-mean changes of the Hadley cell is uncorrelated with precipitation changes in the eastern Mediterranean (Garfinkel et al. 2020a). Moreover, Byrne and O'Gorman (2015) found that modifying the "Wet-Get-Wetter, Dry-Get-Drier" scaling (Held and Soden 2006) to account for changes in horizontal temperature gradients, while relaxing the assumption of fixed relative humidity, improves estimates of regional changes in P-E, especially over land. Therefore, the zonally pronounced drying in the Mediterranean and the strongly correlated change in sea level pressure (SLP) require an explanation including zonally asymmetric factors.

Several zonally sensitive mechanisms of potential relevance to the Mediterranean drying have been put forward. Simpson et al. (2016) show that future precipitation trends over western North

America are regulated by changes in the characteristics of Northern Hemisphere (NH) stationary waves. Strengthened zonal mean westerlies in the sub-tropical upper-troposphere, associated with the warming of the tropical upper-troposphere (a robust and well-studied climate change feature), lead to a lengthening of intermediate-scale zonally propagating stationary waves. This lengthening results in a shift of the meridional winds in the Pacific Ocean, directly altering precipitation patterns in the western US via drying northerlies and wetting southerlies. The CMIP5 multi-model mean response analyzed in Simpson et al. (2016) suggests a downstream effect of the Pacific lengthening over the Atlantic Ocean and Eurasia, although models with a larger response over North America do not necessarily show the same over the Mediterranean. Moreover, different processes and time-scales of the climate response to increasing GHGs have been found to constrain hydro-climate changes in the South-West US versus the Mediterranean (Zappa et al. 2020). The relevance of this mechanism for Mediterranean drying will be investigated in section 5a.

Gervais et al. (2019) analyse the atmospheric response to an idealized North Atlantic Warming Hole (NAWH), the warming deficit in the sub-polar North Atlantic sea surface temperatures seen both in 20th century observations (Rahmstorf et al. 2015) and in future climate projections (Drijfhout et al. 2012; Gervais et al. 2018). They find that the enhanced SST gradient caused by the NAWH leads to a stronger sub-polar SST front. This generates increased surface baroclinic transient eddy activity that propagates vertically and downstream. In the upper-troposphere, this eddy activity enhances the mid-latitudes eddy-driven jet well downstream of the NAWH. Consistent with geostrophic balance, this is associated with equivalent-barotropic increased (reduced) geopotential height equatorwards (polewards) of the jet change. The relevance of this regional circulation response to warming for Mediterranean climate will be discussed in sections 5c and 6b.

Tuel and Eltahir (2020) argue that a weakening of the land-sea temperature gradient in the Mediterranean region accounts for a considerable fraction of the projected drying in the region. Specifically, enhanced warming over land compared to sea, expected as CO_2 concentrations rise (Sutton et al. 2007), reduces the winter temperature gradient between the Mediterranean sea and the land surrounding it. The geostrophically balanced response to the decreased gradient leads to a surface anticyclonic circulation, suppressing winter precipitation. The importance of this mechanism will be assessed in section 5d.

Finally, Zappa et al. (2020) propose that in regions where atmospheric circulation is important for hydro-climate changes, the precipitation response to warming should be characterized using three timescales: a rapid adjustment to the change in radiative forcing, a fast sea-surface temperature (SST) driven response, and a slow SST-driven response. The warming pattern differs for each time-scale and each induces different circulation changes. They find that the precipitation decline in the Mediterranean evolves in quasi-equilibrium with GHG forcing and is largest in the fast SST-driven response. Moreover, only in response to this time-scale does a strong surface anticyclonic circulation form, suggesting a dominant role for circulation changes forced by the fast SST response. This is not the case in all Mediterranean-like regions. In the US west coast for example, where a significant wetting is projected as GHG concentrations rise (Neelin et al. 2013), the full hydro-climate response reaches its maxima only after GHG concentrations stabilize, and the projected wetting is largely due to the slow SST-driven response. This framework and the strong decline in Mediterranean precipitation in the fast SST-driven response helps inform the design of the experiments performed in this paper.

3. Data and Methods

All simulations presented in this paper are run using the Model of an Idealized Moist Atmosphere (MiMA), an intermediate-complexity general circulation model (Jucker and Gerber 2017; Garfinkel et al. 2020c,b). A key advantage of the model is that it captures the interplay between atmospheric dynamics, radiation, and moisture, but with idealizations that allow mechanisms to be isolated. The model simulates the primitive equations on the sphere at moderate resolution, generating realistic synoptic variability. It uses the RRTMG radiation scheme, developed by Atmospheric and Environmental Research (AER) (Iacono et al. 2008), which allows us to incorporate the radiative impacts of ozone and water vapor into the model. The hydrological cycle and a boundary layer scheme based on Monin–Obukhov similarity theory are incorporated following Frierson et al. (2006). The atmosphere is coupled to a mixed-layer ocean and both idealized surface topography and realistic topography configurations are used. The depth of the mixed layer can be varied to approximate land-sea contrast (LSC), and steady east-west ocean heat fluxes (E-W OHF) can be imposed to approximate heat transport by ocean currents (Garfinkel et al. 2020c,b).

The flexible setup of the physical parameterizations allows one to perturb the climate state without extensive re-tuning. Specifically, the addition of orography, LSC, and E-W OHF can be switched on or off independently. Hence, in a single modeling framework, we can alternately simulate a moist zonally symmetric aqua-planet or a model that can compete with CMIP6 models in its ability to simulate both the zonal mean and zonal asymmetries of the large-scale atmospheric circulation (Garfinkel et al. 2020c,b), as well as desired states in between. For example, the ability to "turn off LSC", by modifying the mixed layer heat capacity, surface friction and moisture availability, but otherwise retain all other forcings that drive stationary waves, allows us to confirm/deny the importance of LSC changes for the circulation response to warming in the Mediterranean region. This will allow us to assess the relative Mediterranean cooling theory proposed by Tuel and Eltahir (2020). We are thus able to isolate, and subsequently synthesize, fundamental physical processes that regulate the extra-tropical circulation response to GHGs, and more specifically, the response in the Mediterranean basin. Finally, this idealized model has been shown to capture the key processes that drive stationary waves, and the linear and non-linear interaction between them (Garfinkel et al. 2020c).

Many past studies of the response of stationary waves to warming have used stationary wave models linearized about a prescribed zonal mean basic state (Stephenson and Held 1993; Joseph et al. 2004; Freitas and Rao 2014; Simpson et al. 2016) to understand the response. Such a framework allows one to differentiate between the contribution of an altered zonal-mean basic state vs. changes to the zonally asymmetric wave forcings, such as an altered diabatic heating source. Some have found that the response to warming is dominated by changes to zonally asymmetric forcing (Stephenson and Held 1993; Freitas and Rao 2014) while others concluded that the zonal-mean basic state is an important (Joseph et al. 2004), if not the primary driver (Simpson et al. 2016), of the response. A limitation of our modelling framework is that we cannot distinguish these mechanisms, or account for the relative contribution of the basic state versus the zonally asymmetric diabatic heating for the stationary wave response to warming, as the model solves the full non-linear primitive equations, with moisture. This limitation also has its advantages, however, as the zonal asymmetric diabatic tendencies, and to a smaller extent, the zonal-mean flow, are themselves modified by stationary waves (Held et al. 2002), interactions that are captures by the model.

a. Experiments

Table 1 lists the experiments analyzed in this paper. For all configurations, we first run an experiment with contemporary CO2 concentrations, set to a constant 390 ppm (hereafter 1xCO2). For this experiment, we retain the last 37 years after discarding 28 years of spinup. Next, we spin-off from the 29th year of the 1xCO2 simulation and impose an instantaneous quadrupling of CO2 concentrations (1560 ppm; hereafter 4xCO2), and run for an additional 40 years. We examine the last 37 years of this 4xCO2 run. The rationale behind this set up is that all 1xCO2 experiments begin with an equilibrated temperature field, while all 4xCO2 experiments simulate the"fast ocean" response to rising GHGs, similar to the fast-SST response responsible for Mediterranean drying in Zappa et al. (2020, see section 2). This short to intermediate term response is also the one our model is most suited to, as it lacks a deep ocean. All experiments are run at a horizontal resolution of triangular truncation 42 (T42) with 40 vertical pressure levels. Results for each simulation are averaged over 37 equally-weighted years. All results shown in this paper focus on the winter months, chosen to be December-March (DJFM).

The precipitation, temperature and geopotential height field response to a quadrupling of CO2 concentrations are first examined in a realistic climate simulation (experiment 1 in table 1; hereafter ALL), with all three stationary wave drivers present: orography, E-W ocean heat fluxes, and land-sea contrast. When imposed together, these three forcings reproduce the time mean geopotential height field and its zonal deviations (i.e., the stationary waves), as well as CMIP5 models (Garfinkel et al. 2020c). Hence, we refer to them as the building blocks of stationary waves. To evaluate the change in the forcing exerted by each building block as GHG concentrations rise, we run three simulations in which one is deactivated (experiments 2-4 in table 1), and then compare the result to the response in ALL. This yields the "full" nonlinear response, following the terminology of Held et al. (2002), as opposed to the "isolated" nonlinear response, which corresponds to the perturbation obtained by imposing a given building block on an initially zonally symmetric state. This guarantees that the forcing attributed to each individual building block represents not only the change in zonal asymmetries it causes in isolation, but also the linear and non-linear interaction with the background state set up by the other two forcings. A zonally symmetric aqua planet simulation is included for reference (experiment 0 in table 1). In experiments 5-8 the land-mask is

TABLE 1. MiMA Experiments, with "Y" indicating a forcing is on and "N" indicating a forcing is off. The full nonlinear response to any single forcing is the difference between the realistic simulation (experiment 1) and a single negative experiment, i.e. an experiment in which the examined forcing is off. In experiments 5-8 the land-mask was manipulated yet all stationary wave forcings are activated.

Table 1: MiMA Model experiments

Name	Experiment num.	Orography	Land-sea contrast	E-W ocean heat-fluxes	Land-mask manipulation
Aqua planet	0	N	N	N	N
ALL	1	Y	Y	Y	N
No ocean heat-fluxes	2	Y	Y	N	N
No land-sea contrast	3	Y	N	Y	N
No orography	4	N	Y	Y	N
No Mediterranean Sea	5	Y	Y	Y	Mediterranean Sea changed to land
No North Africa & no Europe	6	Y	Y	Y	Europe & North Africa changed to sea
No Asia	7	Y	Y	Y	Eurasian continent changed to sea
No North America	8	Y	Y	Y	North America changed to sea

manipulated, allowing us to evaluate the role of regional and hemispherical LSC elements for the stationary wave response.

The difference between "land" and "ocean" is in the heat capacity, surface friction, and moisture availability. For the realistic experiment, observed orography as resolved by the model at T42, is applied. In experiments in which the effect of orography is deactivated, a uniform height of just 15 [m] is used over land areas. E-W ocean heat fluxes include idealized Pacific and Atlantic Ocean tropical warm pools, and an approximation of northern hemisphere western boundary currents: the Gulf Stream in the western Atlantic and Kuroshio in the western Pacific. The ocean horizontal heat transport adds no net heat to the ocean. For a detailed description of the representation of horizontal heat transport, orography and parameterization of land vs. ocean, please see Garfinkel et al. (2020c).

b. Zonally anomalous steady-state thermodynamic budget

Stationary wave amplitude and structure, and hence their response to a warming climate, depend greatly upon zonal-asymmetries in diabatic heating and the meridional temperature gradient (Charney and Drazin 1961; Hoskins and Karoly 1981), both of which are expected to change in response to warming. This effect can be interpreted and quantified through the zonally anomalous steady-state thermodynamic budget, which following Wills and Schneider (2018) and Garfinkel et al. (2020c) can be written as:

$$\left(\underbrace{\overline{u}\frac{\partial\overline{\theta}}{\partial x}}_{\text{zonal advection}} + \overbrace{\overline{v}\frac{\partial\overline{\theta}}{\partial y}}^{\text{meridional advection}} + \underbrace{\overline{\omega}\frac{\partial\overline{\theta}}{\partial p}}_{\text{vertical term}} \right)^* + \overbrace{\nabla\cdot(\overline{\mathbf{v}'\theta'})^*}^{\text{transient eddies}} - \underbrace{\overline{Q}^*}_{\text{diabatic terms}} = 0 \qquad (1)$$

where θ is the potential temperature, ω is the vertical pressure velocity and Q is the diabatic heating due to latent heat release, radiation, and other non-conservative processes. Time means are denoted by bars, deviations from a zonal mean are denoted by an asterisk, and deviations from the time mean are denoted by primes. The first three terms on the LHS mark the temperature advection by the time-mean flow and $\nabla\cdot(\overline{\mathbf{v}'\theta'})^*$ is the temperature fluxes by transient eddies.

Extra-tropical diabatic heating is balanced primarily by horizontal advection rather than by adiabatic heating and vertical motion (Hoskins and Karoly 1981; Held 1983). If the horizontal advection term includes a contribution from meridional temperature advection, then the implied meridional winds necessitate a stationary wave response. The amplitude of this stationary wave response is sensitive to the magnitude of $d\theta/dy$, and hence altered $d\theta/dy$ in response to climate change also affects the net stationary wave response. Specifically, a weakening (in absolute magnitude) of the meridional temperature gradient $d\theta/dy$ requires a stronger stationary wave, i.e., meridional wind $\overline{v}$, to restore balance, absent any other changes (Wills et al. 2019; Held et al. 2002). Moreover, changes in the zonal temperature gradient $d\theta/dx$ also force changes in meridional temperature advection.

To further illustrate the forcing of stationary waves, the zonally anomalous steady-state thermodynamic (Eq.2) can be rearranged, as in (Garfinkel et al. 2020c):

$$\left(\overline{v}\frac{\partial\overline{\theta}}{\partial y}\right)^{*} = -\left(\overline{u}\frac{\partial\overline{\theta}}{\partial x}+\overline{\omega}\frac{\partial\overline{\theta}}{\partial p}\right)^{*} - \nabla\cdot(\overline{\mathbf{v}'\theta'})^{*}+\overline{Q}^{*} = 0 \tag{2}$$

The budget in equation 2 will be utilized in section 5c to gain further understanding of our results and particularly, of the stationary wave response to changes in the spatial pattern of temperature.

c. Metrics

Wills et al. (2019) describe differences between several commonly used stationary wave metrics. The atmospheric circulation is often represented by the horizontal stream-function. Assuming geostrophic balance (appropriate if the focus is on the extra-tropics), the circulation can equally be represented by geopotential height on a constant pressure surface. Both of these metrics capture the rotational element of the flow, but not the divergent component (Wills et al. 2019). To consider both rotational and divergent elements of the stationary wave together, zonal anomalies of horizontal winds (either u or v) can be used. We choose to quantify the planetary stationary wave as the time mean deviations from zonal mean of the geopotential height field, as it has been strongly associated with Mediterranean drying in past studies (Giorgi and Lionello 2008; Zappa et al. 2015b). The stationary wave response in the main experiments in this paper is essentially the same if diagnosed by the meridional wind v* (see Figs.S1-S3 in the supplemental material), with no significant difference in the results and interpretation.

Planetary scale stationary waves are principally forced near the surface, and then propagate vertically upwards (Charney and Drazin 1961). Winter NH stationary waves are largely barotropic, with the largest anomalies in the mid-upper troposphere. Therefore we choose to present changes to the stationary waves at 230hPa, while changes to the temperature field and the zonally anomalous thermodynamic budget are diagnosed at 700hPa.

4. The precipitation and circulation response to warming in the Mediterranean region and the role of stationary wave building blocks

The change in winter precipitation following a quadrupling of CO2 concentrations is presented in Figure 1 for experiments 0-7 of table 1. The percentage noted in bold on each figure quantifies the precipitation change in the eastern half of the Mediterranean basin (29-40N, 19-40E), projected to experience the most enhanced drying in winter months (Giorgi and Lionello 2008; Brogli et al. 2019). A decrease in precipitation is found over most of the subtropics in the realistic configuration with all three forcings activated (ALL, Fig. 1a). A strong and zonally pronounced drying is found over the Mediterranean Sea and the land surrounding it, with a difference in magnitude between the north-west and south-east of the basin, consistent with previous studies (Giorgi and Lionello 2008; Brogli et al. 2019; Tuel and Eltahir 2020).

In the zonally symmetric aquaplanet configuration, with all three stationary wave drivers deactivated, there is only moderate drying in the subtropics (Fig. 1b). In the zonal mean, ALL exhibits substantially more drying: 29% between 29-40N, vs. just 2% in the aquaplanet. While all three stationary waves building blocks encourage subtropical drying, pronounced drying in the Mediterranean in particular is strongly tied to changes in the E-W OHF and LSC-driven waves (Fig. 1c-d). When either of these two building blocks is deactivated, approximately 30% less Mediterranean drying is found compared to ALL. In contrast, when orographic stationary waves are removed, their is little change to the precipitation response to warming in the region (Fig. 1e).

The magnitude and pattern of future subtropical precipitation changes have been found to vary widely across models and are sensitive to convection scheme and parameterization (Garfinkel et al. 2024). The large scale circulation response, however, is a more robust feature associated with Mediterranean drying. Therefore we will focus the rest of this paper on the changes in the geopotential height in the Mediterranean region, a variable with higher reliability in GCMs in general, and in our more idealized model in particular (Garfinkel et al. 2020c).

Fig. 2 displays the zonally asymmetric response of the upper-tropospheric geopotential height field to a quadrupling of CO2 concentration in our experiments. The stationary wave in ALL with contemporary CO2 concentrations is very similar to that in the historical simulation of CMIP5 models, as detailed by Garfinkel et al. (2020c). The stationary wave change in response to a quadrupling of CO2 concentrations in ALL is also very similar to the end of century projections

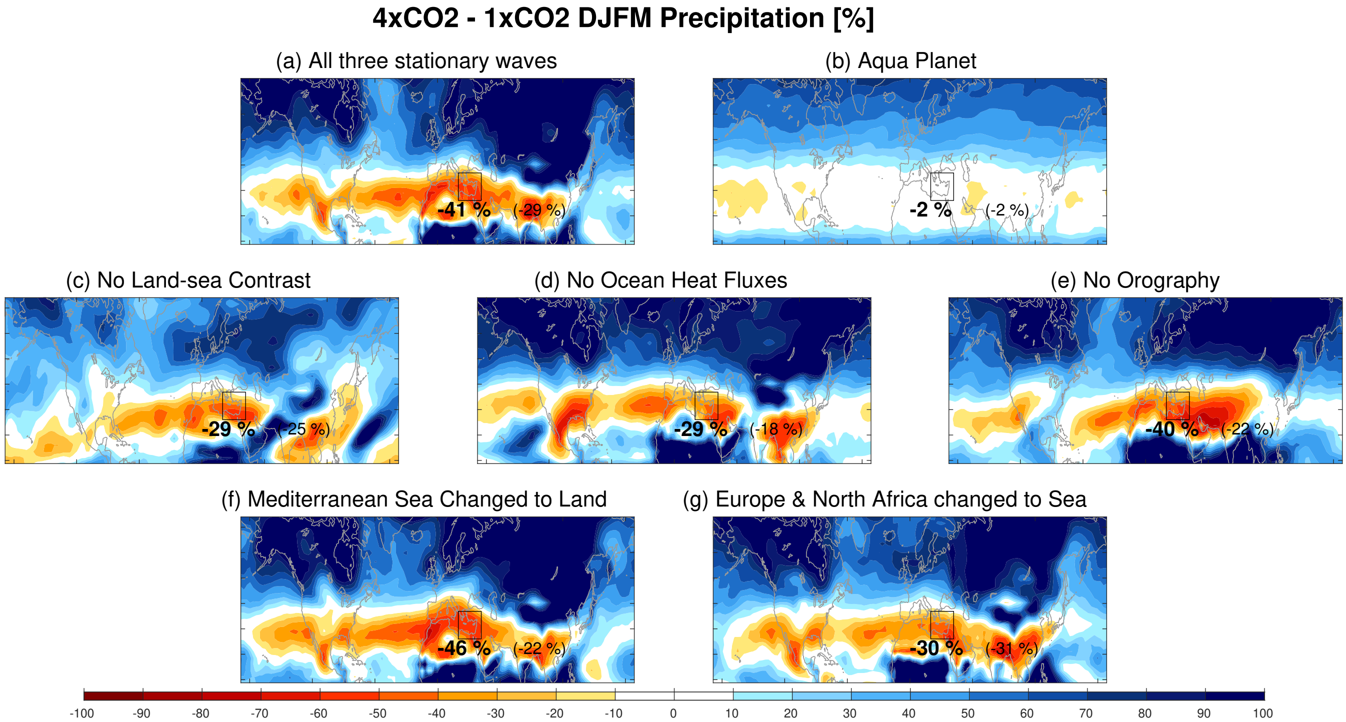

FIG. 1. DJFM percentage change in precipitation 4xCO2-1xCO2 for (a) the realistic configuration with all three stationary wave building blocks; (b) aquaplanet configuration with none of the building blocks; (c) orography and E-W OHF only; (d) orography and LSC only; (e) LSC and E-W OHF only; (f) Mediterranean Sea changed to land; (f) Europe & North Africa changed to sea. Noted in bold on each subplot is the precipitation change in the eastern half of the Mediterranean basin (29-40N, 19-40E; outlined). In brackets is the zonal-mean drying for the same latitude band (29-40N).

in the RCP8.5 scenario averaged over CMIP5 models (Wills et al. 2019). Some discrepancies are found in the east Pacific sector and along the south-western north American coast. These are regions where future precipitation projections are less robust due to model-based uncertainty (Seager et al. 2024).

The first order NH stationary wave response to warming is a down-stream shift in phase of the mid-latitude wave (Fig. 2a lower panel). This response is more pronounced, and with larger meridional span, in the Atlantic sector compared to the Pacific sector. The Western North America ridge and Hudson Bay trough strengthen with warming, while the East Asian low weakens slightly. Focusing on the Mediterranean region, the climatological 1xCO2 east-Atlantic ridge shifts eastwards in phase in response to 4xCO2 while maintaining its amplitude, generating a strong anti-cyclonic

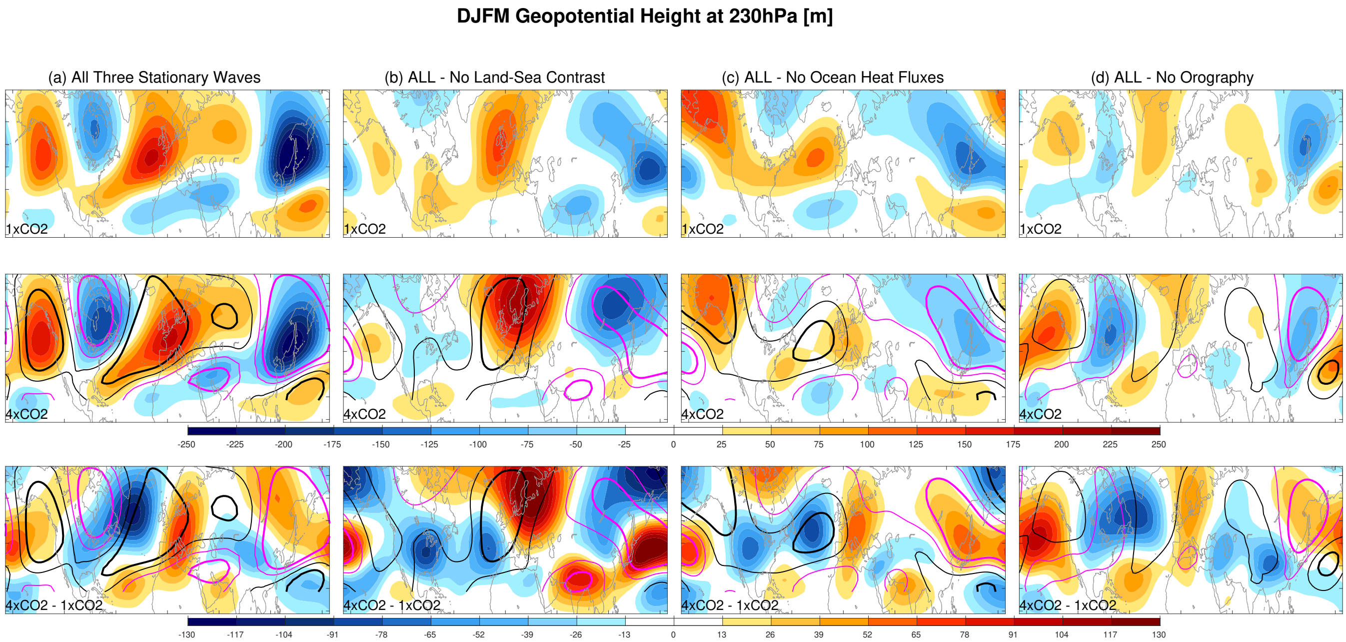

FIG. 2. DJFM zonally anomalous geopotential height at 230hPa for (a) the realistic configuration with all three stationary wave building blocks (ALL); (b) ALL - (orography + E-W OHF); (c) ALL - (orography + LSC); (d) ALL - (LSC + E-W OHF). The first row is the 1xCO2 climatology (shading). The second row is the 4xCO2 climatology (shading) compared to the 1xCO2 climatology (contours). The third row is the 4xCO2-1xCO2 anomaly (shading) compared to the 1xCO2 climatology (contours). The zonal-mean geopotential height at each latitude is subtracted to form deviations from the zonal-mean, and we then time average each of the 1xCO2 and 4xCO2 responses, before computing their difference.

anomaly across the center of the Mediterranean Sea and stretching north over western-central Europe, consistent with previous studies (Giorgi and Lionello 2008; Wills et al. 2019; Tuel and Eltahir 2020). This upper-tropospheric anomaly over the Mediterranean in response to warming is not a result of changes in synoptic-scale variability, as we find very similar results when using a 10-day low pass filter (Fig. S4 in the supplemental material), though transient eddies do contribute to barotropizing the anomaly, as will be shown in section 5c.

We next decompose the stationary wave pattern into the response to each of the three stationary wave drivers (Fig. 2b-d). We present the stationary wave generated in experiments 2-4 as the difference between ALL and each experiment, isolating the full non-linear response to each building block (for the direct results of experiments 2-4 see Fig. S5 of the supplemental material).

The warming response of the stationary wave forced by LSC (Fig. 2b) is complex, as expected given the detailed spatial pattern of the SST response to warming (Zappa et al. 2020). Focusing on the Euro-Atlantic sector, the North Atlantic ridge is strongly amplified and shifted downstream and poleward. This causes a strong positive anomaly over northern Europe, altering the location and meridional extent of the Mediterranean ridge. The Mediterranean ridge itself, however, seems more directly forced by the other two building blocks.

The warming response of the stationary wave forced by zonal ocean heat flux (Fig. 2c) is a weakening and downstream shift. This phase shift is pronounced primarily in the north-east Atlantic, generating a positive anomaly over the Mediterranean, similar in its spatial pattern to that in ALL, and accounting for approximately 65% of its amplitude.

The response of the stationary wave forced by orography to warming (Fig. 2d) is a strengthening of the wave over the Pacific Ocean and North America and a weakening over Asia. The wave driven by the Himalayas and Tibetan Plateau weakens, while the wave forced by the Rocky Mountains strengthens and expands zonally. The latter results in a positive anomaly downstream over north-western Europe and the western Mediterranean Sea, which also contributes to the response in ALL (approximately 35% of the response in Fig. 2a).

Changes in the stationary wave forced by E-W OHF can account for a significant part of the amplitude and location of the anomalous Mediterranean ridge, with a more modest contribution from the orography forced wave. The LSC-driven wave does not generate a clear anti-cyclonic signal above the Mediterranean, although it does further north, affecting the final position of the ridge (Fig. S5b in the supplemental material further clarifies this point, showing the location of the ridge in the simulation with no LSC).

An important caveat is that the sum of the responses to each of the three building blocks does not yield the total stationary wave in the 1xCO2 (as shown by Garfinkel et al. (2020c)), 4xCO2, or 4xCO2-1xCO2 rows in Fig. 2. A similar result is found when considering the sum of the precipitation responses to each of the building blocks in figure 1. This non-additivity highlights the substantial nonlinear interactions in the system. Therefore we can't simply reduce the problem to a linear combination of forcings. It is for this reason that we do not consider the isolated response to each of the building blocks in this paper. This also implies that mechanisms found in linearized stationary wave models may not translate to a more complex GCM, let alone the real atmosphere.

In light of the non-additive dynamic between the stationary wave forcings, the decomposition of the stationary wave response to the relative contribution of the basic state and the zonally asymmetric diabatic heating, as performed in studies with linear baroclinic stationary wave models (Stephenson and Held 1993; Joseph et al. 2004; Freitas and Rao 2014), is not very meaningful.

5. A process oriented assessment of the circulation response to warming over the Mediterranean

Despite the non-additivity of the precipitation and circulation responses to stationary wave building blocks in a warmer climate, a reductionist, process-oriented approach can still identify and quantify key drivers and mechanisms of the response. To do so, in the following section we perform a wavenumber decomposition of the stationary wave response to warming (sub-sections 5a, 5b), utilize the zonally anomalous steady-state thermodynamic balance (5c) and explore the forcing of changes in several regional LSC components (5d).

To clarify the mechanisms behind the stationary wave changes, we distinguish between large-scale (k $\leq$ 3) and intermediate-scale (k $\geq$ 4) stationary waves. The former propagate more meridionally, while the latter propagate zonally and are generally meridionally trapped by midlatitude waveguides. Fig. S8 in the supplemental material clarifies the different character of these scales, showing the climatological stationary wave as a function of zonal wavenumber in MiMA, following figure 4c of Simpson et al. (2016).

a. The intermediate-scale (zonal wavenumber 4-7) stationary wave response

According to the linear theory of barotropic Rossby waves in a zonal-mean flow (Hoskins and Karoly 1981; Hoskins and Ambrizzi 1993; Held et al. 2002), the background flow influences the stationary waves through the total wavenumber K_s, which can be written:

$$K_s = (k^2 + l^2)^{1/2} = \left(\frac{\beta - \overline{u}_{yy}}{\overline{u}}\right)^{1/2} \qquad (3)$$

where k is the zonal wavenumber, l is the meridional wavenumber, β is the meridional gradient of absolute vorticity and $\overline{u}$ is the time-mean zonal wind (equations 2.4 and 2.7 of Hoskins and Ambrizzi 1993). Strengthened upper-tropospheric $\overline{u}$ (which is a direct response to strengthened mid- and upper-tropospheric meridional temperature gradients driven by increased CO2) reduces the barotropic Rossby wavenumber K_s, altering the mid-latitude wave guide. Stationary waves can adapt by reducing the zonal wavenumber k (Simpson et al. 2016). A change in the wave-guide in the form of a reduced Rossby wave number primarily affects the structure of intermediate-scale waves, inducing lengthening and propagation further downstream. This mechanism was applied to the Pacific-North American sector by Simpson et al. (2016) and we now assess its relevance to the Euro-Atlantic sector.

Figure 3 shows the geopotential height at 230 hPa for stationary waves with zonal wavenumber 4-7, the intermediate-scale zonally propagating modes expected to zonally elongate in response to warming (waves 4-5 are preferred, while waves 6-7 are weakened; Simpson et al. 2016). While there is evidence for this lengthening effect in some sectors, it is not evident in others. Over East-Asia and the north-east Pacific, a small downstream phase shift is found, consistent with Simpson et al. (2016), together with a slight weakening of the nodes. Over North America the first order response is an equatorward shift in phase. A zonal downstream phase shift and strengthening is found between $\sim$ 20-40N, crossing the Atlantic ocean, while further north over North America the wave weakens significantly and the phase response isn't clear (see also Fig. S3 in the supplemental material for the response in v*). In the Euro-Atlantic sector, on the northern flank of the Mediterranean Sea (40-60N), the 4xCO2 wave is in opposite phase to the 1xCO2 wave, making it difficult to determine with certainty the direction of the shift. To the south, over North Africa and the Arabian Peninsula (20-40N) the phase stays the same and only the amplitude strengthens. A strong positive anomaly is generated over the Mediterranean in these intermediate-scale waves, stretching north over central Europe, similar in location to the full wave response (Fig. 2a), albeit weaker.

We next decompose the intermediate-scale stationary wave into the response of each of its three drivers (Fig. 3b-d). The wave forced by LSC exhibits a clear downstream phase shift and weakening over all of the NH mid-latitudes, with a significantly larger shift in the Euro-Atlantic nodes. The weakening of the wave is expected, as the LSC generally weakens in a warmer climate (Sutton et al. 2007).

The intermediate-scale wave forced by E-W OHF shifts equatorward with warming and strengthens between 20-40N. On the other hand, between 40-60N the 4xCO2 wave is of opposite phase

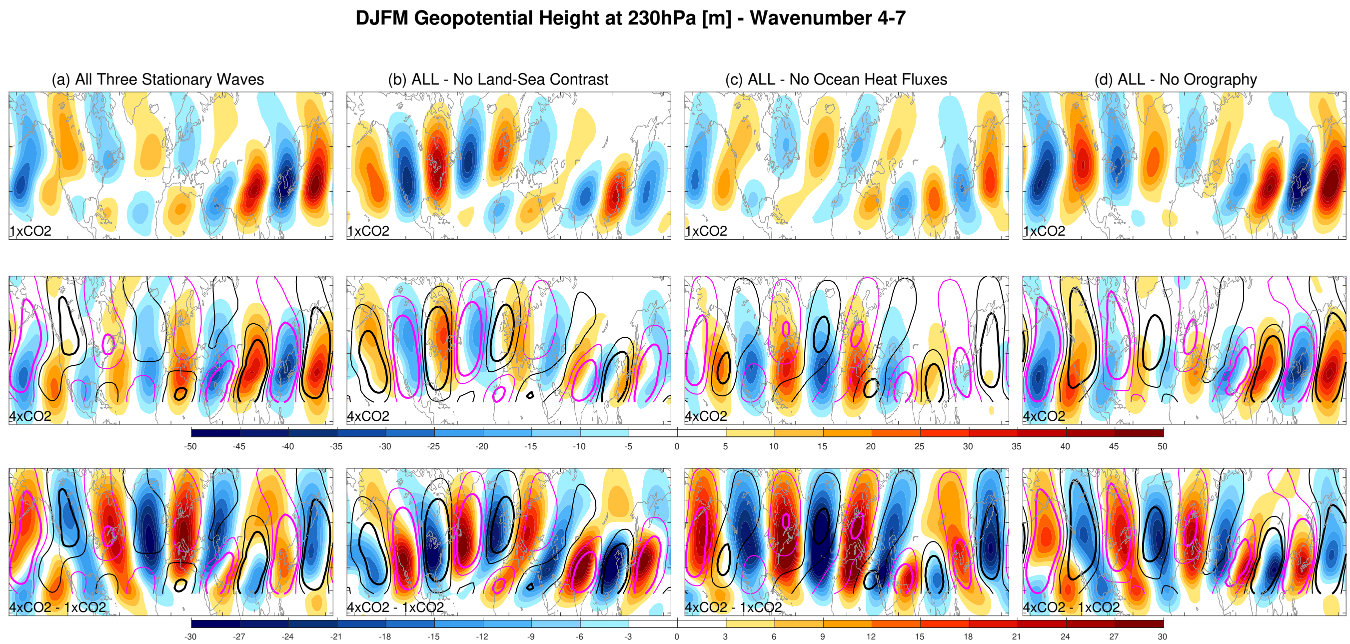

Fig. 3. As in Fig. 2, but for wavenumbers 4-7.

to the 1xCO2 wave, again making it difficult to determine whether the wave shifts downstream or upstream with warming. Exceptions are found in east-Asia and the west-Pacific, where the main response is a weakening of the wave.

For orography-forced waves, an upstream and equatorward shift in phase is found downstream of the Rocky Mountains and across the western half of Eurasia, resulting in a positive anomaly over the Mediterranean. Downstream of the Himalaya and Tibetan Plateau and across the Western and Central Pacific, no phase shift is found. The nodes upstream of the Rocky Mountains in the East Pacific shift equatorward. An overall weakening of the wave is seen throughout the majority of the mid-latitudes and subtropics, with some exceptions to be discussed in section 6c.

Overall, the lengthening mechanism of intermediate-scale waves in response to warming (Simpson et al. 2016) varies zonally and meridionally and is most apparent with the LSC forced wave, but not the orography forced wave. A potential explanation for this difference lies in the mechanical forcing of orography vs. the thermal forcing of LSC, and the opposite response of the waves to an altered low-level zonal wind speed (Held and Ting 1990), as discussed in section 6c. The positive pressure anomaly over the Mediterranean in response to changes in intermediate-scale waves (Fig. 3a) is a non-linear response of the regional signature of these separate components, and accounts for approximately 35% of the full response over the Mediterranean (Fig. 2a). This suggests further mechanism(s) are involved in the stationary wave change over the Mediterranean and the Euro-Atlantic sector.

b. The large-scale stationary wave response to warming

We next assess the change in stationary waves with zonal wavenumber 1-3, the large-scale meridionally propagating modes, separating wavenumbers 1-2 from wavenumber 3 due to key differences between them. Figure 4 shows the change in zonal wavenumbers 1-2. The ridge over Europe, both in the present and future climate, is primarily associated with these wavenumbers (note the difference in color scale with Fig. 3). As the climate warms, essentially all nodes strengthen in mid-latitudes, while in the subtropics over Africa/Asia the wave weakens (Fig. 4a), consistent with CMIP5 model mean response in RCP8.5 (Wills et al. 2019). The Euro-Atlantic ridge strengthens and expands, resulting in a positive anti-cyclonic anomaly over the Mediterranean sea, Europe, and North Africa. The Hudson Bay low also strengthens and expands into the North Atlantic. This strengthening in response to 4xCO2 is clearest in the two Atlantic sector nodes, suggesting a regional mechanism. When decomposing the response into the different stationary wave drivers (Fig. 4b-d) we find that the northern European anomaly is primarily due to changes in the LSC-driven wave, while the E-W OHF driven wave forces a large part of the anomaly over central and southern Europe and the Mediterranean Sea, with orography also contributing. As before, the sum of the changes from each of the building blocks does not even qualitatively resemble the total change in ALL.

The stationary wave of zonal wavenumber 3 propagates both zonally and meridionally (Fig. 5). As the climate warms the wave shifts downstream in phase, chiefly zonally, but also meridionally, and largely retains its amplitude. With 1xCO2 concentrations the amplitude and spatial pattern of wave-3 in the mid-latitudes are dominated by the influence of orography. As the climate warms, the orography-forced wave strengthens slightly and shifts down-stream in the zonal direction, similar to the total response. The E-W OHF driven wave weakens and shifts downstream as well, and the LSC-driven wave weakens considerably, with no zonal shift. The weakening of the LSC driven wave is consistent with reduced land-sea contrast in a warmer world. Thus the response of wave-3 to warming is unique for each driver, with the overall response a non-linear superposition of the

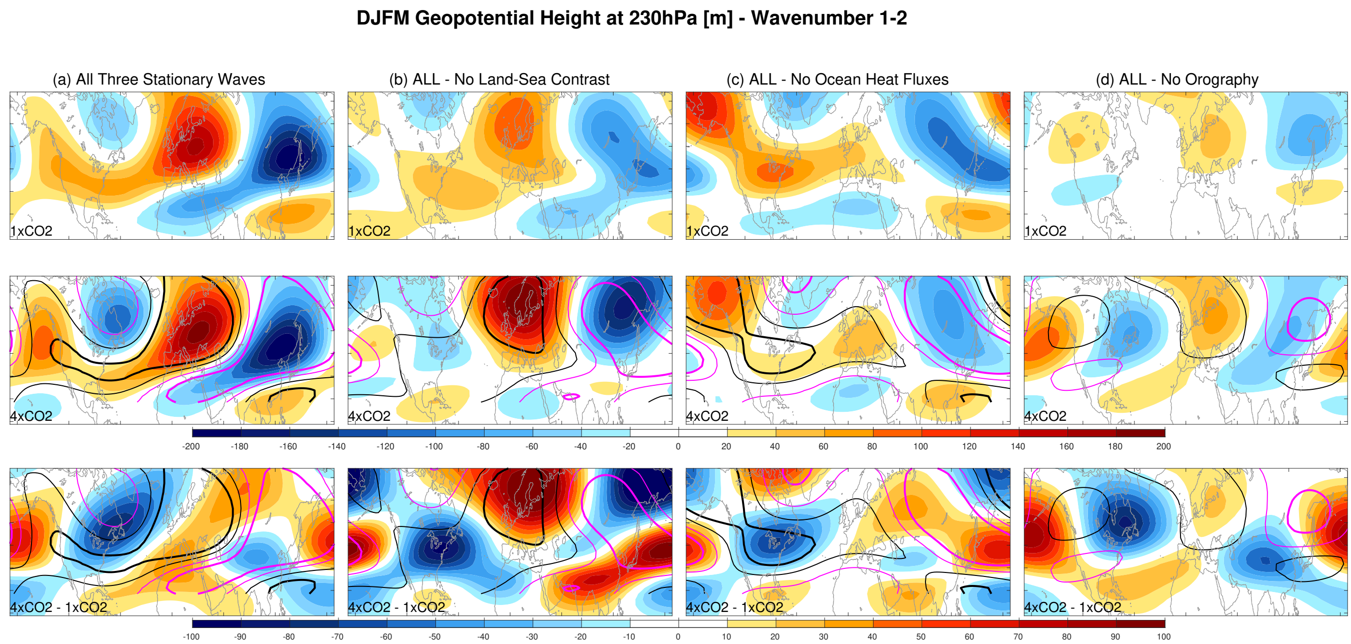

FIG. 4. As in Fig. 2, but for wavenumbers 1-2.

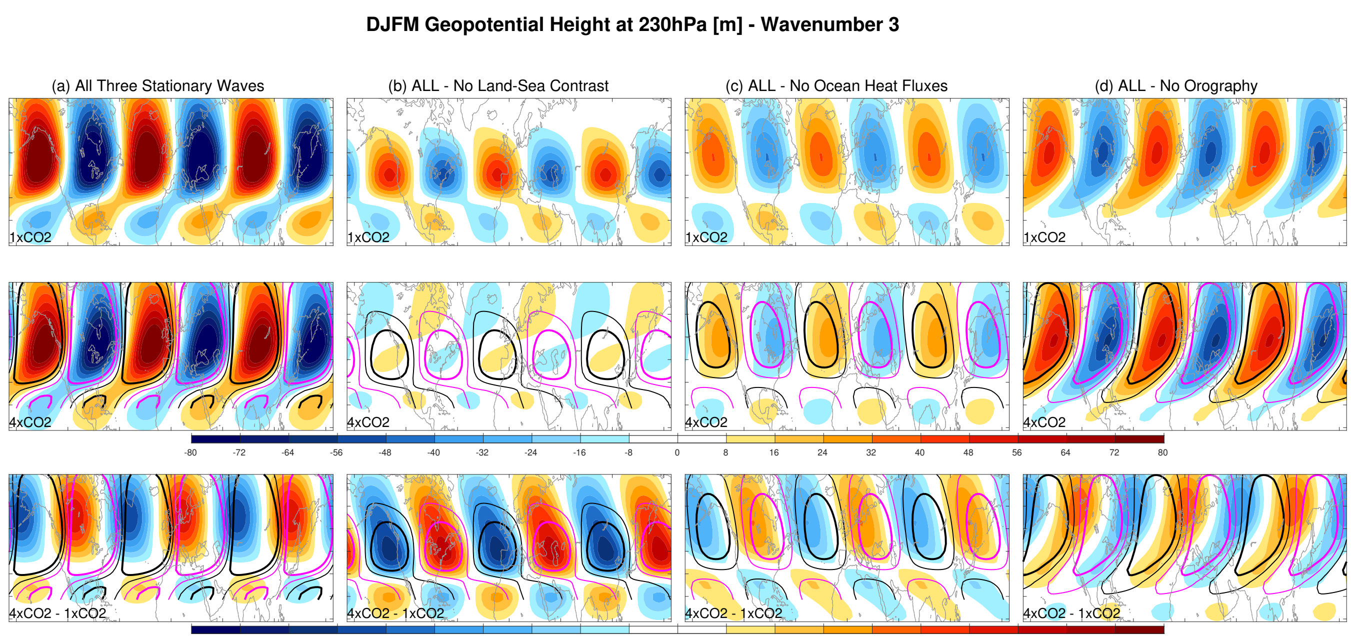

FIG. 5. As in Fig. 2, but for wavenumber 3.

three, amounting to 35-40% of the positive response to the north of the Mediterranean Sea in Fig. 2.

In order to explain this downstream shift of wave-3, we consider the horizontal group velocities of stationary Rossby waves (Hoskins and Karoly 1981):

$$c_{g,x} = \frac{2\overline{u}k^2}{k^2+l^2} \quad \text{and} \quad c_{g,y} = \frac{2\overline{u}kl}{k^2+l^2} \tag{4}$$

where $\overline{u}$ is the zonal mean zonal wind, k the zonal wave number and l the meridional wave number. Increased $\overline{u}$ can result in larger zonal group velocity, so that wave activity can travel further east of the source before it is dissipated. This is consistent with the phase shift in both the zonal and meridional direction of wave-3 in response to warming. Results are similar if we consider the Rossby wave phase speed rather than group velocity.

The mechanism and forcings governing the change in stationary wave-3 in response to warming are different to the large-scale waves 1-2 and intermediate-scale waves 4-7. While the non-linearity of the problem does not allow a full physical interpretation of this response, the phase shift of wave-3 contributes significantly to the anomalous ridge over the Mediterranean in response to warming, especially on the northern flank.

c. Changes to the temperature field and the zonally anomalous steady-state thermodynamic budget

The zonally-anomalous, steady-state thermodynamic balance can be used to understand mechanistically how changes in the temperature gradients, vertical wind, and zonal wind translate to changes in stationary waves. We compute the thermodynamic terms at 700 hPa, as global stationary waves are principally forced near the surface and then propagate vertically upwards, especially for large wavelength (Charney and Drazin 1961). (For changes to the temperature field at 230 hPa for experiments 1-4, see Fig. S9 in the supplemental material.) We first examine the changes to the temperature field induced by the three stationary waves building blocks (Fig. 6), as these are the foundation for explaining the stationary wave changes using the thermodynamic budget. The two main zonally anomalous features in the NH mid-latitudes in response to warming in the Atlantic sector are enhanced warming over land compared to sea, expected as the climate warms (Sutton et al. 2007), and the North Atlantic Warming Hole (NAWH). The two adjacent features generate a large cold temperature anomaly (relative to the overall warming) upstream of the geopotential height anomaly over the Mediterranean (Fig. 6a). In our model environment, enhanced land

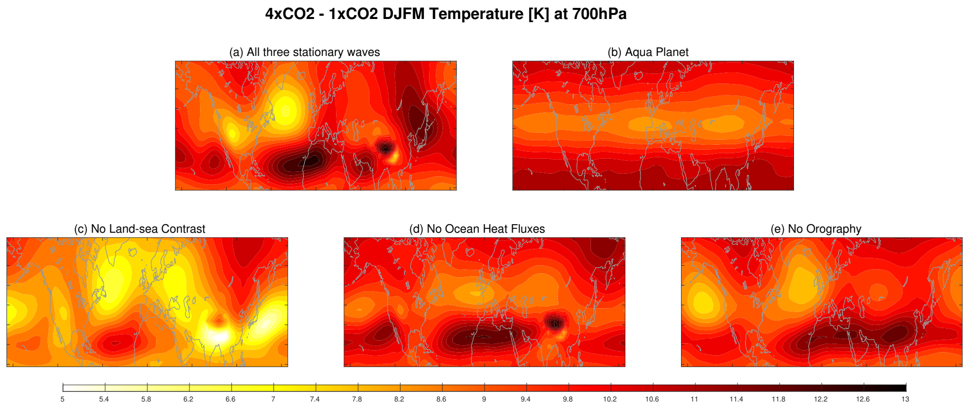

FIG. 6. DJFM 4xCO2-1xCO2 temperature change [K] at 700hPa for (a) ALL; (b) aquaplanet configuration with none of the building blocks; (c) orography and E-W OHF only; (d) orography and LSC only; (e) LSC and E-W OHF only

warming vs. the oceans and the NAWH are tied to two of the stationary wave building blocks, LSC and E-W OHF, respectively (Fig. 6c-d).

The implications of these temperature changes, and in particular of the associated $\frac{\partial\overline{\theta}}{\partial x}$, can be clarified using the the zonally anomalous steady-state thermodynamic balance (Eq. 2), shown in Fig. 7 for ALL. The budget is essentially closed, with negligible residual (see Fig. S10 in the supplemental material). With contemporary 1xCO2 concentrations, all terms in the budget contribute, but the leading order balance is between the zonal and meridional advection terms. The vertical term is important near topographic features, with significant cooling (heating) up-slope (down-slope) of large mountain ranges. The diabatic heating term exhibits a land/sea dipole pattern, in line with the winter land-sea temperature contrast. The transient eddy heat fluxes are downstream of the zonal advection anomalies. As one looks at higher altitudes, the transient and diabatic terms weaken and the balance between the zonal and meridional advection terms dominates (see Fig. S11 in the supplemental material).

As the climate warms, a large, cold zonal advection anomaly is seen in the eastern North Atlantic, spreading inland along the European Atlantic coast (Fig. 7b, bottom). Downstream, over Eastern Europe, is a warm anomaly, with smaller zonal and similar meridional extent. These anomalies are chiefly balanced by the meridional advection in response to warming, which is of opposite phase to the zonal advection (Fig. 7a, bottom). The meridional heat advection anomalies are consistent with the location of the geopotential height anomaly in Fig. 2a. Warm vertical

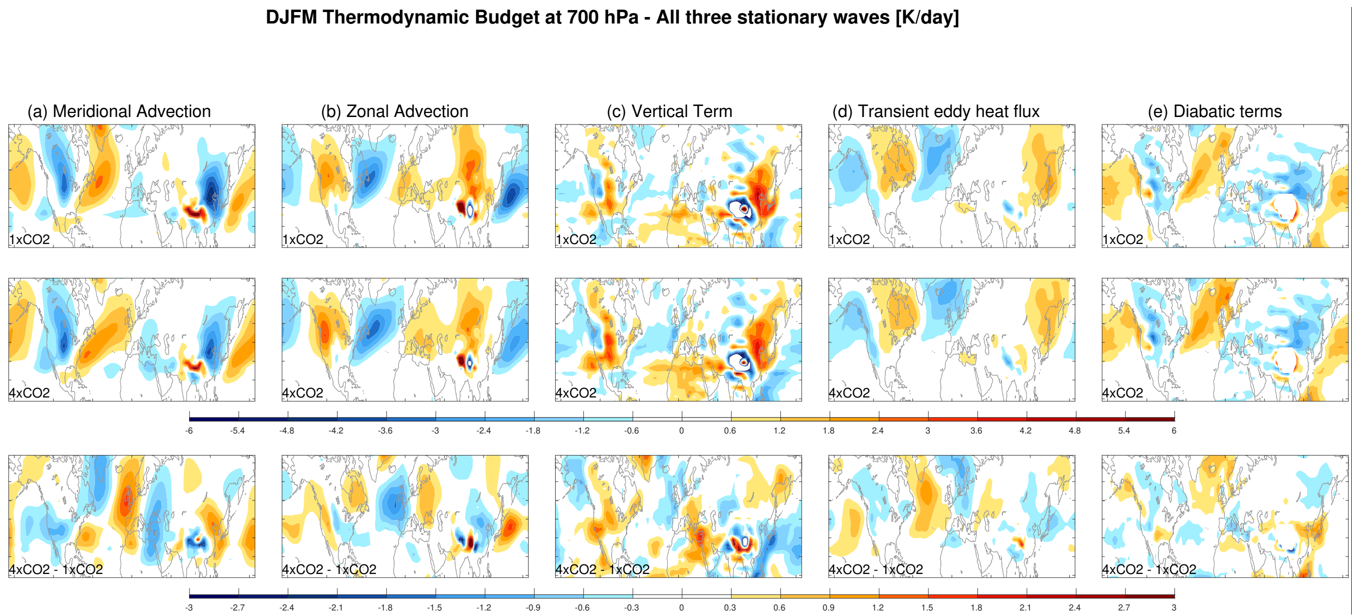

FIG. 7. DJFM zonally anomalous steady-state thermodynamic budget (eq. 1) at 700hPa for the ALL experiment, displaying: (a) meridional advection; (b) zonal advection; (c) vertical term; (d) heat fluxes by transient eddies; (e) diabatic heating due to latent heat release, radiation, and other non-conservative processes. The top and middle rows show results from the 1xCO2 and 4xCO2 integrations, and the final row, their difference.

advection anomalies can be seen in the eastern Mediterranean, partially balancing the temperature change brought about by meridional northerly advection. Transient eddy heat fluxes also play an important role in the response to warming, with positive anomalies above and poleward of the cold zonal advection anomaly in the North Atlantic, transmitting the anomaly upward in the vertical. In the upper-troposphere the positive transient eddy anomaly above the North Atlantic weakens considerably and the zonal and meridional advection terms strengthen (Fig. S11 in the supplemental material). When further decomposing the transient eddy heat fluxes convergence term into the 3-D components, we find that the zonal transient eddy convergence $\nabla \cdot (\overline{\mathbf{u}'\theta'})^*$ contributes the major part of the positive anomaly above the North Atlantic, with positive meridional transient eddies $\nabla \cdot (\overline{\mathbf{v}'\theta'})^*$ as well (Fig. S13 in the supplemental material).

The zonal advection anomaly in response to warming in our experiments can be further decomposed as:

$$\Delta\left(\overline{u}\frac{\partial\overline{\theta}}{\partial x}\right) \approx \Delta\overline{u}\frac{\partial\overline{\theta}}{\partial x}_{1xCO2} + \overline{u}_{1xCO2}\Delta\frac{\partial\overline{\theta}}{\partial x} \tag{5}$$

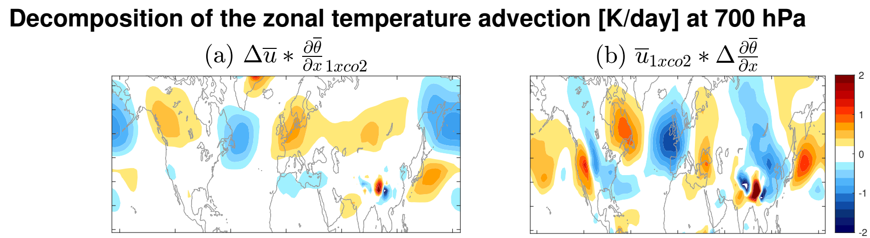

FIG. 8. Zonal advection term of the zonally anomalous steady-state thermodynamic budget decomposed into (a) the forcing exerted by the change in zonal-mean zonal wind; (b) the forcing exerted by the change in the zonal temperature gradient, as in eq. 5. Δ denotes the difference between 4xCO2 and 1xCO2.

where Δ is the difference between 4xCO2 and 1xCO2. This isolates the relative contribution of changes to the time-mean zonal wind $\overline{u}$ and the zonal temperature gradient $\frac{\partial\overline{\theta}}{\partial x}$ for the cold zonal advection anomaly in the eastern North Atlantic and along the European Atlantic coast. In this decomposition we neglect the "Δ-Δ" term, yet the approximation is quite good, as it is still in the linear regime. An altered zonal temperature gradient $\frac{\partial\overline{\theta}}{\partial x}$ in response to warming generates a cold zonal advection anomaly over the north-east Atlantic and western Europe (Fig. 8b), similar in amplitude to the zonal advection anomaly in the thermodynamic budget (Fig. 7b) and slightly larger in zonal extent. In contrast, the influence of the accelerated $\overline{u}$ in the absence of an altered zonal temperature gradient would be to further warm the Euro-Atlantic coast and western Europe (Fig. 8a).

We deduce that the cause of the large cold zonal advection anomaly in the North Atlantic in response to warming (Fig. 7) is the altered zonal temperature gradient $\frac{\partial\overline{\theta}}{\partial x}$, not $\overline{u}$. When performing a similar decomposition of the meridional advection anomaly in response to warming we find the change is dominated by changes in $\overline{v}$, altering the stationary wave (see Fig. S14 of the supplemental material). The net effect is that changes in the zonal temperature gradient $\frac{\partial\overline{\theta}}{\partial x}$ are the most important factor balancing the changes in v*, and these changes in $\frac{\partial\overline{\theta}}{\partial x}$ are in turn associated with the NAWH and the land-sea gradient in warming between Europe and the Atlantic.

While the zonally anomalous thermodynamic budget helps identify the key role of $\frac{\partial\overline{\theta}}{\partial x}$, it cannot establish causality, i.e., determine which of the terms changes first and which subsequently respond. All the terms must balance each other by construction, and hence one term cannot "force" any others. To tackle this difficulty, we compare the budget for the experiments in which we isolate the

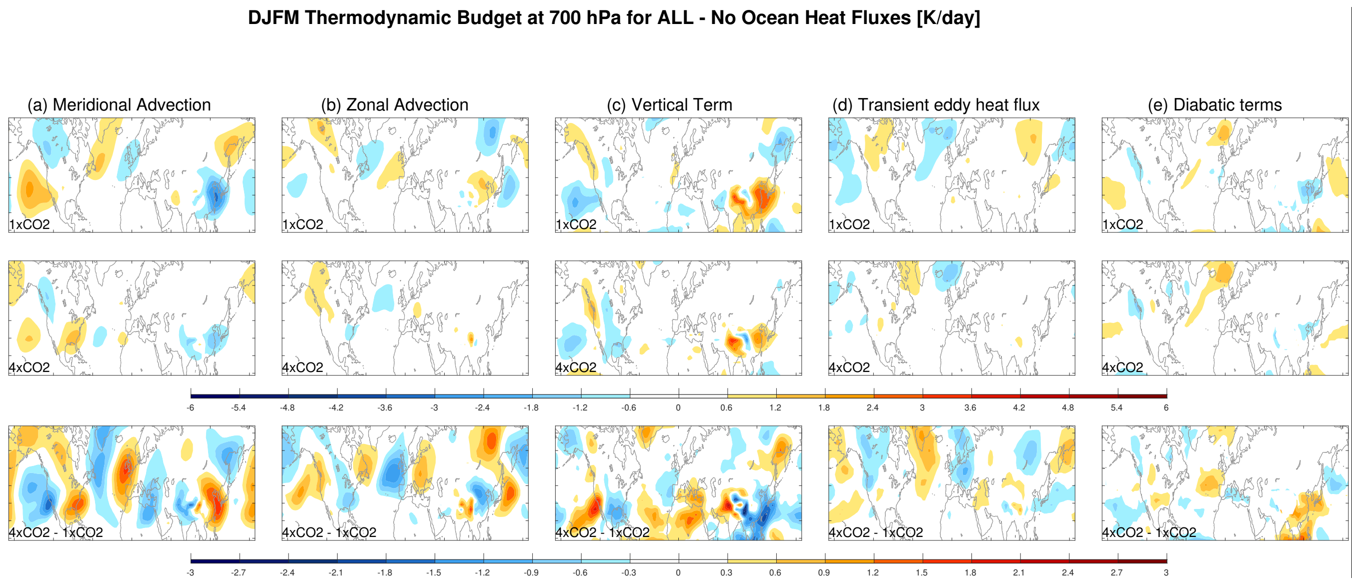

FIG. 9. As in Fig. 7 but for ALL - (orography + LSC).

contribution of LSC and E-W OHF, as changes in both alter the zonal temperature structure in the North Atlantic and Eurasia (Fig. 6).

Figures 9 and 10 show the changes in the thermodynamic budget forced by changes in the E-W OHF and LSC, respectively. The cold zonal advection anomaly found over the eastern North Atlantic and European Atlantic coast in ALL (Fig. 7) appears to stem from a combination of the two. The western and major part of the cold zonal advection anomaly, in the central and Eastern North Atlantic and jutting into Europe, is caused by changes to the E-W OHF (Fig. 9b). The north Atlantic warming hole drives relative cooling in the lower-troposphere north and downstream of the cold SSTs, via a weakening of turbulent fluxes from the ocean to the atmosphere (Fig. 6 and Gervais et al. 2019).

The eastern part of the cold anomaly, along the Atlantic coast and inland into Europe reaching the Adriatic Sea, is caused by altered LSC (Fig. 10b). This can be attributed to the relative cooling of the ocean with respect to land as the climate warms (Sutton et al. 2007), weakening the thermal zonal gradient and therefore cooling the winter warm zonal advection from the Atlantic Ocean into Europe. The western and eastern parts of the transient eddy heat flux anomaly are in turn caused by LSC and E-W OHF respectively (Fig. 10d,9d).

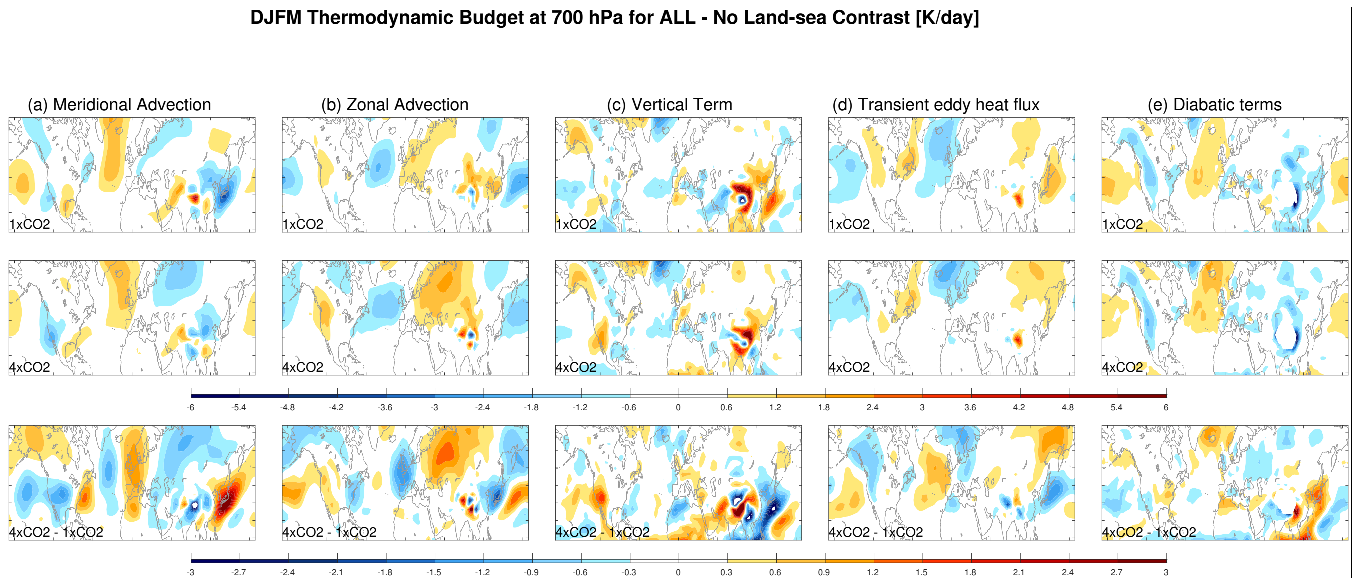

FIG. 10. As in Fig. 7 but for ALL - (orography + E-W OHF)
.

d. Relative Mediterranean cooling and regional land-sea contrast components

Land-sea contrast is an important factor for the development of the ridge over Europe (Fig. 2b), and in this section we aim to understand which specific continent and/or water body is most responsible for this effect. Motivated by the results of Tuel and Eltahir (2020, see Section 2), we first consider the role of the Mediterranean Sea. Specifically, we manipulate the land-mask such that the Mediterranean Sea is changed into land, leaving everything else the same (Fig. 11b). The stationary wave response to 4xCO2 associated with this infilling of the Mediterranean is shown in Figure 12b. A ridge develops over the Mediterranean in response to increased CO2 (Fig. 12b), but it is confined to the south and with a small zonal extent, and far weaker amplitude, relative to the full response in Figure 2. Paradoxically, changing the Mediterranean Sea to land results in enhanced drying compared to the realistic experiment (Fig. 1f).

We next isolate the role of land-sea contrast along the Atlantic coastline with Europe and North Africa by changing all of Europe and North Africa to sea (Fig. 11c). The geopotential height response to the altered Atlantic coast gradient (Fig. 12c) is larger compared to the Mediterranean gradient, and qualitatively captures the response to changes in LSC (Fig. 2b). A similar change in precipitation is found as well (compare panels c & g in Fig. 1), suggesting that in terms of regional

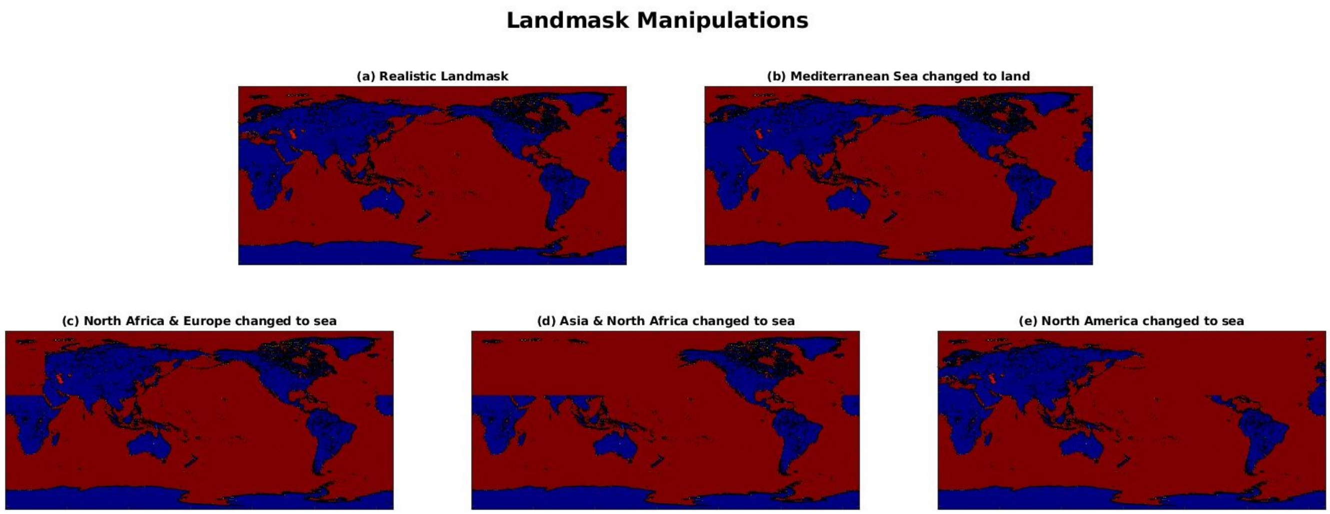

FIG. 11. Landmask manipulation for experiments 5-8 in table 1: (a) Realistic landmask; (b) Mediterranean Sea changed to land; (c) Europe & North Africa changed to sea; (d) Eurasia changed to sea; (e) North America changed to sea.

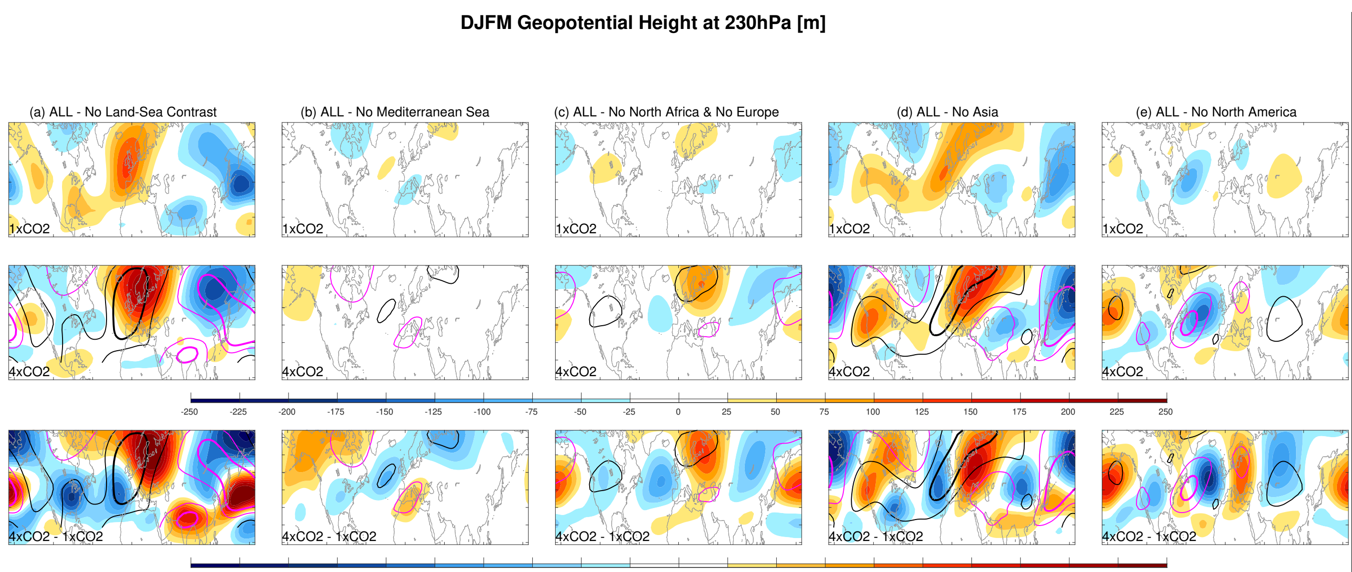

FIG. 12. As in Fig. 2 but for (a) ALL - (orography + E-W OHF); (b) ALL - Mediterranean Sea changed to land; (c) ALL - Europe & North Africa changed to sea; (d) ALL - Eurasia changed to sea; (e) ALL - North America changed to sea.

LSC components, it is the Atlantic coast, not the altered Mediterranean gradient, which matters most for the projected drying.

Further experiments to isolate the role of the northern hemisphere continents within the LSC-forced stationary wave response to warming establish the minimal role of relative Mediterranean cooling for future Mediterranean drying. The bulk of the response of the LSC-forced stationary wave in the Euro-Atlantic region stems from an altered gradient between the Atlantic Ocean and the land to the east of it, with some adjustment caused by a wave-train propagating from North-America (Fig. 12d,e). This point is further apparent when examining the low-level stationary wave and its response to various LSC components (Fig. S7 in the supplemental material).

Changes to the NH LSC-forced stationary-wave amplitude in response to warming are dominated by enhanced warming of the Asian continent (Fig. 12d), in line with previous studies (e.g., Portal et al. 2022). Some extrema, such as the strong positive anomalies in the polar North Atlantic and in the North Pacific Ocean, are governed mainly by the relative warming of the North American continent (Fig. 12e). However, these anomalies are generally overpowered by changes forced by the other stationary wave building blocks, and are far weaker in the full stationary wave (Fig. 2a) compared to the forcing exerted by LSC alone (Fig. 2b).

6. Discussion

The three building blocks which ultimately force the stationary waves each exhibit unique responses to warming, and contribute differently to Mediterranean drying. Changes to E-W ocean heat transport have a direct effect on the Mediterranean ridge, via the downstream response to the NAWH. Changes to the LSC act to significantly alter the location, amplitude and meridional extent of the Mediterranean ridge, but are not its underlying cause. Changes in the orography-forced wave are governed by changes in the low-level wind and contribute to Mediterranean drying via an indirect downstream effect of modified wave propagation from large-scale topography. These three interact non-additively, such that one cannot quantify the precise contribution of each to Mediterranean drying. While the non-linearity of the building blocks does not allow a simple decomposition, we have identified three key mechanistic pathways that matter quantitatively, and when combined they drive the stationary wave response over the Mediterranean. Two have appeared in some form in the literature, though typically not in the context of Mediterranean drying. We next discuss further detail and reasoning of the mechanisms, and their regional manifestations.

a. The lengthening response of intermediate-scale stationary waves

Section 5a found evidence for a lengthening response to warming in intermediate-scale stationary waves (Simpson et al. 2016). This lengthening, however, is sector-specific and only present in response to specific stationary wave building blocks. To better understand this zonal structure, we look at the climatological barotropic stationary wavenumber K_s (Fig. 13). In the 1xCO2 simulation a wave-guide, i.e., a local maxima in K_s, exists along the East-Asian coast, stretching east into the Pacific Ocean in the south, and from the subtropical north-east Atlantic eastward through the Mediterranean region to the Caspian Sea (Fig. 13). As the climate warms and the upper-troposheric winds change (see figure S15 in the supplemental material), the wave-guide is no longer found in northeast Asia, yet does remain further south along the Pacific coast. Northeast Asia is the area with the largest decrease in K_s in response to warming (Fig. 13), which appears to destroy the wave guide. This may explain why over North America we see a clear phase shift in waves 4-7 (Fig. 3a) only in latitudes 20-40N, but not further north (40-60N), as in the absence of an upstream wave-guide, the lengthening mechanism is ill-posed (Hoskins and Karoly 1981; Simpson et al. 2016).

Over southeast Asia and the West Pacific coast, and upstream all the way to the Arabian Peninsula, the wave-guide remains in 4xCO2, and the decrease in K_s is weaker than in other regions (compare with northeast Asia, east Atlantic). This may explain why only a small phase shift in seen in East Asia, and the chief response is a weakening of the wave (Fig. 3a).

Upstream of the Mediterranean, the picture isn't clear. The strong phase shift of the wave (Fig. 3a) is matched by a decrease in K_s upstream (Fig. 13), but the upstream wave guide has vanished. A new wave-guide is found in 4xCO2 in northeast North America (Fig. 13), upstream of the strong phase shift in wavenumbers 4-7 north of the Mediterranean (Fig. 3a). In this case, however, it is due to a local increase in K_s and therefore cannot explain the large phase shift over Europe via the lengthening mechanism.

Another approach is to look at regional changes in K_s. We find a good match between areas of large regional and upstream decrease in K_s in figure 13a and areas where we see a significant

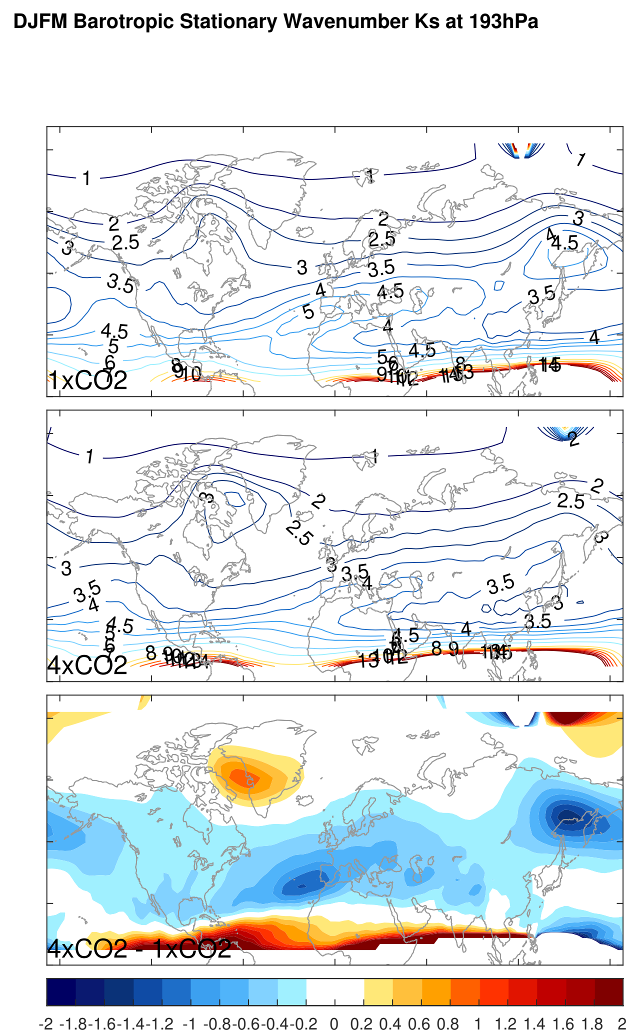

FIG. 13. Barotropic stationary wavenumber K_s at 193 hPa in the ALL experiment, for (a) 1xCO2, (b) 4xCO2 and (c) the difference between b and a.

downstream phase shift of the stationary wave in Figure 3a. In particular, there is a large decrease in K_s both directly over and upstream of the Mediterranean Sea and western Europe, but not for North Africa. The stationary wave phase shifts accordingly, with no shift over North Africa and the Arabian Peninsula and a large shift over Europe and the Mediterranean. Over North America, we see a larger decrease in K_s from 20-40N and less from 40-60N, and the phase shifts follow accordingly. Finally, over East Asia and the northwest Pacific we see a large decrease in K_s in the north and far less to the south, and the phase shift follows again.

b. The role of the North Atlantic warming hole and surface forcing

The response of the winter wavenumber 1-2 stationary waves over the North Atlantic and Europe strongly resembles the mid-tropospheric geopotential-height response downstream to an enhanced winter NAWH and the associated enhanced North Atlantic eddy-driven jet, as isolated by Gervais et al. (2019). In particular, compare Fig. 4a with Fig. 3 of Gervais et al. (2019). This similarity is further demonstrated when comparing the 4xCO2-1xCO2 $v*$ at 230 hPa in our model with the NAWH response of the wind speed at the dynamic tropopause; compare Supplemental Fig. S2 showing the $v*$ wave 1-2 with Fig. 3 of Gervais et al. (2019). Among the three stationary wave drivers in our model, the response to the NAWH in Gervais et al. (2019) can be best compared to the response to altered E-W OHF (Fig. 4c, Fig. S2c in the supplemental material). The zonally anomalous thermodynamic budget illustrates, from a stationary wave perspective, the mechanism by which the NAWH generates a high pressure anomaly downstream in future projections (Fig. 9), complementary to that shown in Gervais et al. (2019). We conclude that the NAWH contributes directly to the anomalous rain-suppressing Mediterranean ridge in future climate projections. Delworth et al. (2022) found that while climate change mitigation can reduce summer drying in the Mediterranean, winter drying continues due to the persistent forcing of a weakened AMOC. A slow-down of the AMOC has been primarily linked to the NAWH (Rahmstorf et al. 2015; Caesar et al. 2018), but a NAWH appears in our model even without a dynamical ocean, as has been shown previously by He et al. (2022).

In addition, the thermodynamic budget demonstrates that the reduced warming of the North Atlantic Ocean relative to Eurasia further enhances the downstream response to the NAWH (Fig. 10). The altered land-sea gradient enhances the zonal gradient of low-level temperature, and thus increases the zonal temperature advection. Most of this change is balanced by a strengthened meridional temperature advection, which necessitates a stronger and downstream shifted North Atlantic ridge (compare Fig. 7 with Figs. 10 and 9). Altered LSC in future climate has been found to cause interference with stationary waves of zonal wavenumbers 1-2 (Portal et al. 2022), in agreement with our results. The altered E-W OHF seem to force the Euro-Mediterranean anomaly directly, while the forcing exerted by changes in LSC impacts the pressure field over a far larger spatial extent, and affects the Mediterranean ridge indirectly.

c. The role of orographic stationary waves in Mediterranean drying

While the two thermally driven stationary waves in our model, associated with LSC and E-W OHF, show a clear and largely explainable contribution to future Mediterranean drying, the role of the orograhically-driven wave is more complex. Climate change leads to a weakening of the orographically forced wave in Eastern Asia above and downstream of the Himalayas and the Tibetan Plateau, yet a strengthened and zonally elongated wave is seen above and downstream of the Rocky Mountains (Fig. 2). The latter results in a strengthening of the ridge over the Mediterranean and western Europe. This response can be better understood by decomposing the wave by length-scale.

A general strengthening of the orographic stationary waves of wavenumber 1-2 is found in response to warming (Fig. 4d). Orography, however, plays a smaller role in waves 1-2 relative to the contribution of the other two building blocks (Fig. 4). It becomes more important for changes in wavenumbers 3-7. The stationary wave forced by orography is of smaller zonal wavelength relative to the thermally-forced ones, both in our model (Fig. 2) and in past studies which decomposed stationary waves using a steady-state model (Held et al. 2002). Therefore, the strengthening of orographic stationary wave 1-2 in our model is likely a non-linear response, and not related to changes in the source of the wave, such as via changes to the stratospheric vortex and vertical wave activity flux (Wang and Kushner 2011; Sun et al. 2015; Wills et al. 2019).

The amplitude and spatial pattern of wave-3 are dominated by the influence of orography, both in 1xCO_2 and in response to climate change (Fig. 5). In a warmer climate, a slight strengthening of the orographic wave-3 is found, but the main response is a zonal and meridional downstream phase shift, similar to the total wave-3 response (Fig 5a,d). This shift in phase may be the result of an increased group velocity in response to enhanced $\overline{u}$, yet it remains unclear why this mechanism is seen only in stationary wave 3, and not in any other wavenumber (not shown). Moreover, orographic waves 4-7 shift upstream in many sectors when grouped together (Fig. 3d), especially downstream of the Rocky Mountains.

While a downstream shift and lengthening is not apparent with the intermediate-scale stationary orographic waves (wavenumber 4-7), a weakening is evident in response to warming (Fig. 3d), in agreement with Wills and Schneider (2018). This response is related to changes in the zonal wind. The amplitude of orographically forced stationary waves is proportional to the velocity of the wind impinging on orography, when using a quasi-geostrophic linear model (Held and Ting 1990), and also in response to warming in a non-linear idealized GCM (Wills and Schneider 2018). In the north Pacific Ocean, upstream of the Rocky Mountains, a poleward shift of the low-level jet is observed in our model, resulting in weaker westerly winds impinging on the mountain range (Fig. 14). Accordingly, downstream of the Rocky mountains we see the largest weakening in the orographically forced intermediate-scale stationary wave (Fig. 3d), with the weakening propagating until Western Europe and forming the northern part of the positive pressure anomaly over the Mediterranean. Upstream of the Himalayas and the Tibetan Plateau we observe a more moderate weakening of the low level winds (Fig. 14), consistent with the moderate weakening of the wave downstream over East Asia and the west Pacific (Fig. 3d).

In areas further from orographic influence, such as in subtropical south-west North America, we see a strengthening of the wave, stretching through the subtropical North Atlantic to North Africa and the Arabian Peninsula. It weakens again further east, as it meets the large orography of East-Asia. This strengthening of the orogaphic wave far from large orography may be due to other factors, such as increased extra tropical static stability and reduced meridional temperature gradients (Wills and Schneider 2018).

Orographic wave-3 lies further north than waves 4-7, centered poleward of the large orography (Fig. 5). The poleward shift of low level winds in a warmer climate generally brings stronger winds to the northern mid-latitudes, in our model (Fig. 14) and in CMIP5 models (Simpson et al. 2014; Wills et al. 2019). This difference in latitude may explain the strengthening of the orography forced wave-3, in contrast to the weakening of the waves forced by LSC and E-W OHF, as the amplitude of orographic waves is proportional to the speed of low level winds, while thermally forced waves vary inversely (Held and Ting 1990).

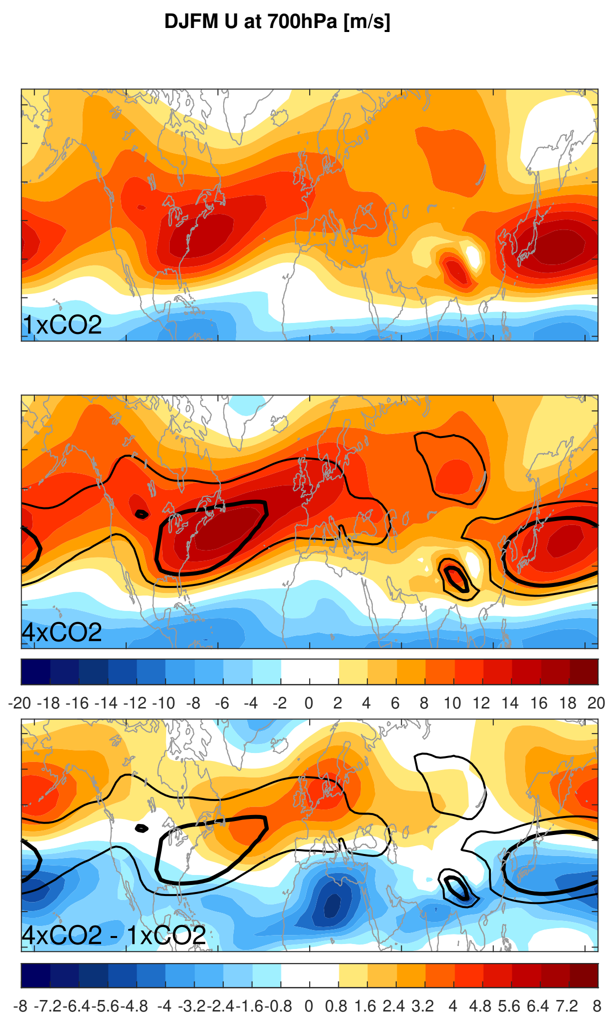

725 FIG. 14. Zonal wind U at 700 hPa in the ALL experiment, for (a) 1xCO2, (b) 4xCO2 and (c) the difference
726 between b and a. Contours in the 2nd and 3rd row are the 1xCO2 climatology from the 1st row.

7. Conclusions

Projected precipitation decline in the Mediterranean is closely tied to changes in NH winter stationary waves. An anomalous, rain-suppressing ridge is projected to develop over the Mediterranean, caused by a combination of several mechanisms. We argue that the three principle mechanisms are:

(a) **Lengthening of intermediate scale stationary waves**: Enhanced subtropical zonal-mean zonal wind aloft elongates and phase shifts waves of zonal wavenumbers 4-7 (Simpson et al. 2016). This mechanism is dominated by changes in stationary waves forced by land-sea contrast and E-W ocean heat transport, yet does not manifest for orographic waves, and is responsible for approximately 35% of the total Mediterranean ridge response (Fig. 3 in section 5a).

(b) **The North Atlantic Warming Hole and Atlantic land-sea contrast**: Large-scale stationary wave anomalies form over western Europe and the North Atlantic, a downstream response to the North Atlantic warm hole (Gervais et al. 2019) and to enhanced warming of the Eurasian landmass relative to the ocean. The joint forcing of these two cold temperature anomalies is captured in the response of wavenumbers 1-2 (Fig. 4 in section 5b). This mechanism is further understood in terms of changes to the zonally anomalous steady-state thermodynamic budget and the consequent stationary wave response, particularly via altered zonal temperature advection (sections 5c,6b). 30-40% of the total ridge is associated with this mechanism.

(c) **The planetery scale orographic wave-3 response to warming**: A downstream phase shift of stationary wave 3 is observed, possibly due to increased group velocity in response to enhanced low-level winds, which causes wave activity to travel further east of the source (Fig. 5 in section 5b). This response is primarily associated with changes in the circulation response to orographic forcing and contributes 35-40 % of the north-western part of the projected Mediterranean ridge. We are not aware of any previous studies linking this mechanism to the Mediterranean ridge.

In our modeling framework, reduced warming of the Mediterranean Sea with respect to land (Tuel and Eltahir 2020) causes a weak anti-cyclonic circulation over the region in response to warming. Its contribution to the large-scale circulation changes and projected drying in the Mediterranean region, however, is much smaller than the three aforementioned effects (Fig. 1f; Fig. 12 in section 5d).

Our results highlight the non-linear and non-additive behavior of the zonally asymmetric circulation response to warming. However, by decomposing this response according to wavenumber, we are able to quantitatively disentangle NH stationary wave changes, identify key mechanisms governing the change, and further clarify the role of large scale circulation changes for the projected drying of the Mediterranean region.

Acknowledgments. BK and CIG acknowledge the support of the Israel Science Foundation (grant agreement 1727/21). CIG and EPG are also supported by the US-Israel Binational Science Foundation (BSF) grant 2020316. EPG acknowledges support from the U.S. NSF through grant OAC-2004572.

Data availability statement. The version of MiMA used in this study, including the modified source code can be downloaded from https://github.com/ianpwhite/MiMA/releases/tag/MiMA-ThermalForcing-v1.0beta (with DOI: https://doi.org/10.5281/zenodo.4523199).

References

Armon, M., F. Marra, Y. Enzel, D. Rostkier-Edelstein, C. I. Garfinkel, O. Adam, U. Dayan, and E. Morin, 2022: Reduced rainfall in future heavy precipitation events related to contracted rain area despite increased rain rate. *Earth's Future*, **10 (1)**, e2021EF002 397.

Brandefelt, J., and H. Körnich, 2008: Northern hemisphere stationary waves in future climate projections. *Journal of Climate*, **21 (23)**, 6341–6353.

Brogli, R., S. L. Sørland, N. Kröner, and C. Schär, 2019: Causes of future mediterranean precipitation decline depend on the season. *Environmental Research Letters*, **14 (11)**, 114 017.

Byrne, M. P., and P. A. O'Gorman, 2015: The response of precipitation minus evapotranspiration to climate warming: Why the "wet-get-wetter, dry-get-drier" scaling does not hold over land. *Journal of Climate*, **28 (20)**, 8078–8092.

Caesar, L., S. Rahmstorf, A. Robinson, G. Feulner, and V. Saba, 2018: Observed fingerprint of a weakening atlantic ocean overturning circulation. *Nature*, **556 (7700)**, 191–196.

Charney, J. G., and P. G. Drazin, 1961: Propagation of planetary-scale disturbances from the lower into the upper atmosphere. *Journal of Geophysical Research*, **66 (1)**, 83–109.

Cos, J., F. Doblas-Reyes, M. Jury, R. Marcos, P.-A. Bretonnière, and M. Samsó, 2022: The mediterranean climate change hotspot in the cmip5 and cmip6 projections. *Earth System Dynamics*, **13 (1)**, 321–340.

Delworth, T. L., W. F. Cooke, V. Naik, D. Paynter, and L. Zhang, 2022: A weakened amoc may prolong greenhouse gas–induced mediterranean drying even with significant and rapid climate change mitigation. *Proceedings of the National Academy of Sciences*, **119 (35)**, e2116655 119.

Drijfhout, S., G. J. Van Oldenborgh, and A. Cimatoribus, 2012: Is a decline of amoc causing the warming hole above the north atlantic in observed and modeled warming patterns? *Journal of Climate*, **25 (24)**, 8373–8379.

Freitas, A. C. V., and V. B. Rao, 2014: Global changes in propagation of stationary waves in a warming scenario. *Quarterly Journal of the Royal Meteorological Society*, **140 (679)**, 364–383.

Frierson, D. M., I. M. Held, and P. Zurita-Gotor, 2006: A gray-radiation aquaplanet moist gcm. part i: Static stability and eddy scale. *Journal of the atmospheric sciences*, **63 (10)**, 2548–2566.

Garfinkel, C. I., O. Adam, E. Morin, Y. Enzel, E. Elbaum, M. Bartov, D. Rostkier-Edelstein, and U. Dayan, 2020a: The role of zonally averaged climate change in contributing to intermodel spread in cmip5 predicted local precipitation changes. *Journal of Climate*, **33 (3)**, 1141–1154.

Garfinkel, C. I., B. Keller, O. Lachmy, I. White, E. P. Gerber, M. Jucker, and O. Adam, 2024: Impact of parameterized convection on the storm track and near-surface jet response to global warming: implications for mechanisms of the future poleward shift. *Journal of Climate*.

Garfinkel, C. I., I. White, E. P. Gerber, and M. Jucker, 2020b: The impact of sst biases in the tropical east pacific and agulhas current region on atmospheric stationary waves in the southern hemisphere. *Journal of Climate*, **33 (21)**, 9351–9374.

Garfinkel, C. I., I. White, E. P. Gerber, M. Jucker, and M. Erez, 2020c: The building blocks of northern hemisphere wintertime stationary waves. *Journal of Climate*, **33 (13)**, 5611–5633.

Gervais, M., J. Shaman, and Y. Kushnir, 2018: Mechanisms governing the development of the north atlantic warming hole in the cesm-le future climate simulations. *Journal of climate*, **31 (15)**, 5927–5946.

Gervais, M., J. Shaman, and Y. Kushnir, 2019: Impacts of the north atlantic warming hole in future climate projections: Mean atmospheric circulation and the north atlantic jet. *Journal of Climate*, **32 (10)**, 2673–2689.

Giorgi, F., 2006: Climate change hot-spots. *Geophysical research letters*, **33 (8)**.

Giorgi, F., and P. Lionello, 2008: Climate change projections for the mediterranean region. *Global and planetary change*, **63 (2-3)**, 90–104.

He, C., A. C. Clement, M. A. Cane, L. N. Murphy, J. M. Klavans, and T. M. Fenske, 2022: A north atlantic warming hole without ocean circulation. *Geophysical Research Letters*, **49 (19)**, e2022GL100 420.

He, J., and B. J. Soden, 2017: A re-examination of the projected subtropical precipitation decline. *Nature Climate Change*, **7 (1)**, 53–57.

Held, I. M., 1983: Stationary and quasi-stationary eddies in the extratropical troposphere: Theory. *Large-scale dynamical processes in the atmosphere*, **127**, 168.

Held, I. M., and B. J. Soden, 2006: Robust responses of the hydrological cycle to global warming. *Journal of climate*, **19 (21)**, 5686–5699.

Held, I. M., and M. Ting, 1990: Orographic versus thermal forcing of stationary waves: The importance of the mean low-level wind. *Journal of Atmospheric Sciences*, **47 (4)**, 495–500.

Held, I. M., M. Ting, and H. Wang, 2002: Northern winter stationary waves: Theory and modeling. *Journal of climate*, **15 (16)**, 2125–2144.

Hoskins, B. J., and T. Ambrizzi, 1993: Rossby wave propagation on a realistic longitudinally varying flow. *Journal of Atmospheric Sciences*, **50 (12)**, 1661–1671.

Hoskins, B. J., and D. J. Karoly, 1981: The steady linear response of a spherical atmosphere to thermal and orographic forcing. *Journal of the atmospheric sciences*, **38 (6)**, 1179–1196.

Iacono, M. J., J. S. Delamere, E. J. Mlawer, M. W. Shephard, S. A. Clough, and W. D. Collins, 2008: Radiative forcing by long-lived greenhouse gases: Calculations with the aer radiative transfer models. *Journal of Geophysical Research: Atmospheres*, **113 (D13)**.

Joseph, R., M. Ting, and P. J. Kushner, 2004: The global stationary wave response to climate change in a coupled gcm. *Journal of climate*, **17 (3)**, 540–556.

Jucker, M., and E. Gerber, 2017: Untangling the annual cycle of the tropical tropopause layer with an idealized moist model. *Journal of Climate*, **30 (18)**, 7339–7358.

Lionello, P., and F. Giorgi, 2007: Winter precipitation and cyclones in the mediterranean region: future climate scenarios in a regional simulation. *Advances in Geosciences*, **12**, 153–158.

Neelin, J. D., B. Langenbrunner, J. E. Meyerson, A. Hall, and N. Berg, 2013: California winter precipitation change under global warming in the coupled model intercomparison project phase 5 ensemble. *Journal of Climate*, **26 (17)**, 6238–6256.

Portal, A., C. Pasquero, F. D'andrea, P. Davini, M. E. Hamouda, and G. Rivière, 2022: Influence of reduced winter land–sea contrast on the midlatitude atmospheric circulation. *Journal of Climate*, **35 (19)**, 6237–6251.

Rahmstorf, S., J. E. Box, G. Feulner, M. E. Mann, A. Robinson, S. Rutherford, and E. J. Schaffernicht, 2015: Exceptional twentieth-century slowdown in atlantic ocean overturning circulation. *Nature climate change*, **5 (5)**, 475–480.

Scheff, J., and D. Frierson, 2012: Twenty-first-century multimodel subtropical precipitation declines are mostly midlatitude shifts. *Journal of Climate*, **25 (12)**, 4330–4347.

Seager, R., N. Naik, and G. A. Vecchi, 2010: Thermodynamic and dynamic mechanisms for large-scale changes in the hydrological cycle in response to global warming. *Journal of climate*, **23 (17)**, 4651–4668.

Seager, R., and Coauthors, 2024: Recent and near-term future changes in impacts-relevant seasonal hydroclimate in the world's mediterranean climate regions. *International Journal of Climatology*.

Simpson, I. R., R. Seager, M. Ting, and T. A. Shaw, 2016: Causes of change in northern hemisphere winter meridional winds and regional hydroclimate. *Nature Climate Change*, **6 (1)**, 65–70.

Simpson, I. R., T. A. Shaw, and R. Seager, 2014: A diagnosis of the seasonally and longitudinally varying midlatitude circulation response to global warming. *Journal of the Atmospheric Sciences*, **71 (7)**, 2489–2515.

Stephenson, D. B., and I. M. Held, 1993: Gcm response of northern winter stationary waves and storm tracks to increasing amounts of carbon dioxide. *Journal of climate*, **6 (10)**, 1859–1870.

Sun, L., C. Deser, and R. A. Tomas, 2015: Mechanisms of stratospheric and tropospheric circulation response to projected arctic sea ice loss. *Journal of Climate*, **28 (19)**, 7824–7845.

Sutton, R. T., B. Dong, and J. M. Gregory, 2007: Land/sea warming ratio in response to climate change: Ipcc ar4 model results and comparison with observations. *Geophysical research letters*, **34 (2)**.

Tuel, A., and E. A. Eltahir, 2020: Why is the mediterranean a climate change hot spot? *Journal of Climate*, **33 (14)**, 5829–5843.

Wang, L., and P. J. Kushner, 2011: Diagnosing the stratosphere-troposphere stationary wave response to climate change in a general circulation model. *Journal of Geophysical Research: Atmospheres*, **116 (D16)**.

Wills, R. C., and T. Schneider, 2018: Mechanisms setting the strength of orographic rossby waves across a wide range of climates in a moist idealized gcm. *Journal of Climate*, **31 (18)**, 7679–7700.

Wills, R. C., R. H. White, and X. J. Levine, 2019: Northern hemisphere stationary waves in a changing climate. *Current climate change reports*, **5**, 372–389.

Zappa, G., P. Ceppi, and T. G. Shepherd, 2020: Time-evolving sea-surface warming patterns modulate the climate change response of subtropical precipitation over land. *Proceedings of the National Academy of Sciences*, **117 (9)**, 4539–4545.

Zappa, G., M. K. Hawcroft, L. Shaffrey, E. Black, and D. J. Brayshaw, 2015a: Extratropical cyclones and the projected decline of winter mediterranean precipitation in the cmip5 models. *Climate Dynamics*, **45**, 1727–1738.

Zappa, G., B. J. Hoskins, and T. G. Shepherd, 2015b: The dependence of wintertime mediterranean precipitation on the atmospheric circulation response to climate change. *Environmental Research Letters*, **10 (10)**, 104 012.